Available online at www.sciencedirect.com
SCIENCE DIRECT
Microporous and Mesoporous Materials 94 (2006) 243–253
MICROPOROUS AND MESOPOROUS MATERIALS
www.elsevier.com/locate/micromeso

Creation of micro and mesoporous Fe^{III} materials utilizing organic template followed by carboxylates exchange for the low concentrations of arsenite removal

Yasuo Izumi [a,*], Dilshad Masih [a], Ken-ichi Aika [a], Yoshimi Seida [b]

[a] *Interdisciplinary Graduate School of Science and Engineering, Tokyo Institute of Technology, Nagatsuta 4259-G1-16, Midori-ku, Yokohama 226-8502, Japan*

[b] *Institute of Research and Innovation, 1201 Takada, Kashiwa 277-0861, Japan*

Received 27 October 2005; received in revised form 24 March 2006; accepted 4 April 2006
Available online 22 May 2006

Abstract

The instability of inorganic framework has been the greatest barrier to synthesize micro and mesoporous $Fe^{III/II}$ materials. This paper uses dodecylsulfate to organize lamellar-structure $FeO_x(OH)_y$ composite followed by smaller carboxylates exchange (formate, acetate, or propionate) to create micropores. XRD, nitrogen sorption/desorption, HR-TEM, FT-IR, ICP, EPMA, TG–DTA, and Fe K-edge EXAFS measurements were used for the characterizations. The lamellar-structure reorganized to wormhole-like framework stabilized with carboxylate anions adsorbed inside micropores. Upon heating at 423 K, a half of acetates/propionates diminished and the specific surface area increased to as much as 230 $m^2\,g^{-1}$. Based on the Fe K-edge EXAFS for $FeO_x(OH)_y$ composite and derivative porous Fe^{III} materials, Fe–O bonds were observed at 2.04–2.09 Å with the coordination number 5–6. Farther Fe···Fe bonds also appeared at 3.21–3.25 Å. The coordination number was obtained to 2–3, reflecting higher dispersion and higher surface area for these porous Fe^{III} materials. The acetate-exchanged $FeO_x(OH)_y$ heated at 423 K exhibited greatest saturated sorption amount ($21\,mg_{As}\,g^{-1}_{adsorbent}$) and equilibrium sorption constant ($1.0 \times 10^7\,ml\,g^{-1}_{As}$) in 0.2–32 ppm of arsenite test solutions among other relevant Fe^{III} materials and Fe^{III} nanoparticles intercalated between clay layers.

Keywords: Iron oxyhydroxide; Carboxylate exchange; Arsenite; Lamellar; Wormhole-like

1. Introduction

Recent regulations concerning the concentration of arsenic in public water supplies are at 10 ppb due to the high carcinogenic risk reported in Bangladesh, West Bengal, Taiwan, Argentina, Vietnam, etc. [1]. Especially, arsenite has fatal effects on human health. For the economic and effective removal of trace amounts of As in drinking water, we recently reported the optimization of Fe^{III} materials for the sorption of low concentrations of As [2]. The screening included α-FeO(OH) with specific surface area (SA) of 16–54 $m^2\,g^{-1}$ [3,4], γ-FeO(OH) with specific SA of 27–176 $m^2\,g^{-1}$, Fe^{3+}-exchanged montmorillonite with specific SA of 46 $m^2\,g^{-1}$, and dispersed $FeO_x(OH)_y$ nanoparticles (average particle size 6 Å) intercalated between montmorillonites with specific SA of 25.8–100 $m^2\,g^{-1}$, in 50 ppb–16 ppm of test As solutions. The uptake capacity on intercalated $FeO_x(OH)_y$ as much as 14 wt.% Fe was the best from both arsenite and arsenate in the equilibrium dissolved As concentration range smaller than 310 ppb [2].

In order to apply them to practical As sorption, further increase of Fe content in sorbents is essential. The superiority of Fe^{III} nanoparticles stabilized between montmorillonite layers was owing to greater equilibrium sorption constant [2]. The As sorption on unsaturated [FeO_6] sites

* Corresponding author. Tel./fax: +81 45 924 5569.
E-mail address: yizumi@chemenv.titech.ac.jp (Y. Izumi).

1387-1811/$ - see front matter © 2006 Elsevier Inc. All rights reserved.
doi:10.1016/j.micromeso.2006.04.002

was stronger and stable. In this paper, highly dispersed Fe^{III} porous materials were synthesized using anionic organic template followed by anion exchange with smaller carboxylates to enable high dispersion and high concentration of Fe in sample simultaneously. Due to the molecular size difference of template and carboxylates anions, micropores were successfully formed.

Fe^{III} inorganic/organic composites were synthesized in the forms of lamellar [5–7], 2-dimensional hexagonal [8], and wormhole-like (holes filled with templates) [9–12]. However, reports are limited that removed the templates by thermal [10–12] or solvent treatment [7–10,12] to effectively form meso or micropores. When the templates were removed, assembled Fe framework decomposed to larger porous structure [12] or fragmented to nanoparticles [9,11]. We discuss the role of carboxylates exchanged and the micro/mesostructure transformation in the heating process. Thus-prepared microporous Fe^{III} materials were applied to the low concentrations of arsenite removal.

2. Experimental section

2.1. Preparation of Fe^{III} porous materials

Fifty milliliters of ferrous chloride (0.10 M) was mixed with 10 ml of sodium dodecylsulfate (0.070 M) at 290 K followed by addition of 10 ml of H_2O_2 (0.25 M) [5–7,13]. The pH value of solution changed from 6 to 3. The Fe^{II} oxidation route was chosen to control moderate rate of solid formation. The solution was stirred for 1 h and filtered. Obtained yellow powder is called $FeO_x(OH)_y$ *composite*. When the molar ratio of Fe^{II} and Na dodecylsulfate was in the range 2:1–1:2 [7], two independent sets of peaks appeared in the X-ray diffraction (XRD) data during treatments. When the ratio was 7:1 as above, all the XRD peak intensity behaved as a single set. Therefore, the ratio was fixed to 7:1.

The $FeO_x(OH)_y$ composite was mixed with 75 ml of sodium formate, acetate, or propionate (0.050 M for each) at 290 K in ethanol [14]. Obtained brown powders are called *anion-exchanged* $FeO_x(OH)_y$. As a control, the $FeO_x(OH)_y$ composite was washed with ethanol [7–10,12] at 290 K. This sample is called *ethanol-washed* $FeO_x(OH)_y$. Each anion-exchanged or ethanol-washed $FeO_x(OH)_y$ was set in furnace in the nitrogen flow with the rate of 40 ml min^{-1}. The temperature was linearly raised from 290 to 523 K with an elevation rate of 2 K min^{-1}.

2.2. XRD, sorption/desorption isotherms, TEM, FT-IR, ICP, EPMA, and TG–DTA measurements

XRD data were obtained using a Multiflex-S diffractometer (Rigaku). Cu Kα emission was used with a Ni filter. The diffractions were monitored in the $2\theta_B$ range of 2–70° (θ_B: Bragg angle). The specific SA was measured at 77 K using a BELSORP Mini (Bell Japan) with N_2 as the adsorbate. The samples were evacuated at 393–423 K for 1 h before measurements. Transmission electron microscope (TEM) observations were performed using field-emission-type JEM-2010 F (JOEL) at the accelerating voltage of 200 kV at the Center of Advanced Materials Analysis (CAMA), Tokyo Institute of Technology (Dr. A. Genseki). The powder was dispersed in carbon tetrachloride using ultrasonic and mounted on carbon-coated Cu grid.

Fe^{III} materials (0.15 g) were thoroughly mixed with KBr powder (IR-grade, Wako) to be 1.0 wt.% Fe and pressed into a disk of 20 mm in diameter. The Fourier-transformed infrared (FT-IR) spectra were measured in transmission mode using Valor III (JASCO) equipped with a MCT detector. The energy resolution was set to 1 cm^{-1}. Nitrogen gas was flowed in sample room to avoid moisture during measurements.

The amounts of $FeO_x(OH)_y$, dodecylsulfate, and formate were based on OH stretching (≈3400 cm^{-1}), CH stretching (2921 and 2852 cm^{-1}), and COO stretching (as, s) (1602 and 1350 cm^{-1}) peaks, respectively (Fig. 4). The amounts of acetate and propionate were based on COO stretching (as, s) peaks (1535 and 1425 cm^{-1}, respectively). The amount of dodecylsulfate was also evaluated based on the stretching peak of sulfate (1226 cm^{-1}). The evaluated amount was essentially identical based on either ν_{CH} or ν_{SO_4} peak. No peaks due to CCO stretching of ethoxyl group were detected at ≈1050 cm^{-1} (as) and 970–870 cm^{-1}(s) [15] for ethanol-washed samples, demonstrating negligible ethanol adsorption on Fe^{III} materials in this paper. These peak areas were compared to corresponding peak areas obtained for diluted α-FeO(OH) disks to 0.1–2.0 wt.% Fe and powder disks to 0.1–2.0 wt.% of dodecylsulfate and Na formate, acetate, or propionate diluted using KBr.

The elemental compositions of Fe, C, O, S, Na, and Cl in acetate-exchanged $FeO_x(OH)_y$ samples were analyzed using inductively coupled plasma (ICP) measurements combined with optical emission spectroscopy (Prodigy, Leeman Labs) and electron probe microanalysis (EPMA) measurements (JXA-8100, Jeol) at CAMA (Dr. T. Toya). LaB_6/W filament was used and the accelerating voltage of incident electrons was 15 kV.

Thermogravimetric differential thermal analysis (TG–DTA) was performed using DTG-60 (Shimadzu) for α-FeO(OH) and acetate-exchanged $FeO_x(OH)_y$. The flow rate of air was 120 ml min^{-1} and the ramping rate of sample was 4 K min^{-1}.

2.3. Fe K-edge XAFS measurements and analysis

The powders of Fe^{III} materials were evacuated at 290 K and transferred to the Pyrex glass cell. The windows were sealed with Kapton film of 12.5 μm in thickness. Sample thickness was controlled to give a Fe K absorption edge jump of 1.0. The Fe K-edge X-ray absorption fine structure (XAFS) spectra were measured in the beamlines 10B and 12 C at KEK-PF in a transmission mode at 20–290 K.

The storage ring energy was 2.5 GeV and the ring current was 437–320 mA. A Si(311) double crystal monochromator was used. N_2 gas and a mixture of N_2 (85%) and Ar (15%) were used in the I_0 and I_t ion chambers, respectively. The rising edge energy of Fe metal was calibrated at 7111.20 eV [16]. The scan steps were ≈0.1, ≈0.5, and ≈2 eV for the pre-edge + edge, post-edge (X-ray absorption near-edge structure: XANES), and EXAFS (extended X-ray absorption fine structure) regions, respectively. The accumulation time for a data point was 1–5 s.

The EXAFS data analysis was performed using XDAP (XAFS Services International) based on works of M. Vaarkamp, H. Linders, and D. Koningsberger. The details were described elsewhere [2]. Multiple shell analyses were performed for the Fourier-filtered k^3-weighted EXAFS data in the k- and R-space using empirical parameters extracted from EXAFS for α-Fe_2O_3 [2]. The bond distances and coordination numbers of Fe–O and Fe···Fe were based on crystal structure data for α-Fe_2O_3 [17,18]. The σ^2 values are relative to those for α-Fe_2O_3. The many-body reduction factor S_0^2 was assumed to be equal for sample and reference. The goodness of fit was given as requested by the Committee on Standards and Criteria in X-ray Absorption Spectroscopy.

2.4. Arsenite sorption tests

Twenty milliliters of 0.2–16 (or 0.2–32) ppm solution of $As_2^{III}O_3$ was introduced to 50 mg of each Fe^{III} material in a 30-ml polypropylene tube. The mixture was shaken at a rate of 130 times min^{-1} at 290 K for 12 h. The system reached an equilibrium within 12 h. The equilibrium dissolved As concentration was determined by ICP measurements.

3. Results

3.1. XRD

The XRD spectra measured for $FeO_x(OH)_y$ composite and the derivative samples were depicted in Fig. 1. Obtained d spacing values based on the diffraction angle were summarized in Table 1. In the XRD spectrum for $FeO_x(OH)_y$ composite (Fig. 1A(a)), strong, medium, and weak peaks were observed centered at $2\theta_B = 2.44°$, 4.9°, and 7.6°, respectively. These were assigned to (001), (002), and (003) diffractions, respectively, of lamellar-structure [5–7,19] with d spacing of 36.2 Å.

The spectrum A(a) changed by carboxylate anions exchange. When formate was used, all peaks became too weak (Fig. 1A(b)). When acetate and propionate were used, a broad peak appeared centered at $2\theta_B = 4.5°$ (A(c, d); corresponding d spacing 20 ± 2 Å). These peaks were not due to the (002) diffraction for lamellar-structure because corresponding (001) diffraction peak anticipated to appear at $2\theta_B = 2.3°$ was not observed. For the ethanol-washed $FeO_x(OH)_y$, a medium peak appeared at $2\theta_B = 3.2°$ (A(e); d spacing 28 ± 1 Å).

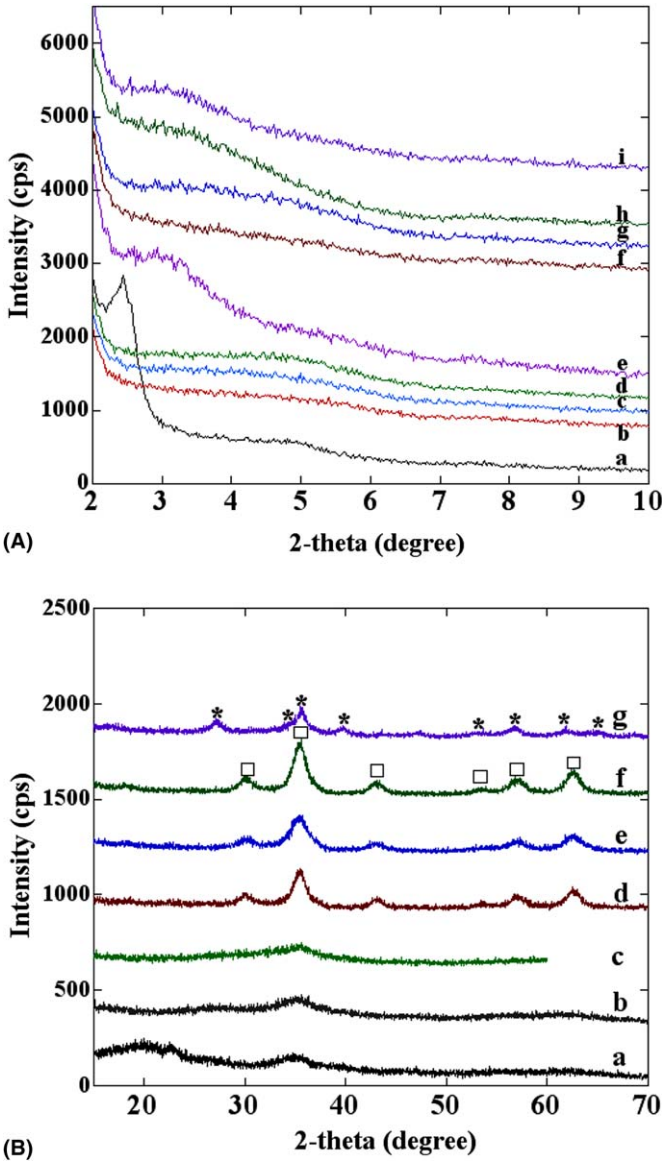

Fig. 1. XRD spectra. (A) Lower angle region measured for $FeO_x(OH)_y$ composite (a), formate, acetate, and propionate-exchanged $FeO_x(OH)_y$ (b–d, respectively), ethanol-washed $FeO_x(OH)_y$ (e), and b–e heated at 423 K (f–i, respectively). (B) Higher angle region measured for $FeO_x(OH)_y$ composite (a), acetate-exchanged $FeO_x(OH)_y$ (b), b heated at 423 K (c), formate, acetate, and propionate-exchanged $FeO_x(OH)_y$ heated at 533 K (d–f, respectively), and ethanol-washed $FeO_x(OH)_y$ heated at 533 K (g). (*) Peaks derived from FeO(OH) (PDF No.03-0440); (□) peaks derived from Fe_3O_4 (ICSD No. 36314, PDF No. 75-0033).

When these samples were heated at 423 K, the broad peaks for acetate/propionate-exchanged samples shifted downward to 4.4° (Fig. 1A(g)) and 3.9° (h), respectively. These angles corresponded to the d spacings of 20 ± 2 and 23 ± 2 Å (Table 1g and h). The peak at $2\theta_B = 3.2°$ for ethanol-washed sample remained at the same angle (Fig. 1A(i)). The peak intensity deceased to one third. When these samples were heated at 533 K, all the peaks disappeared in the $2\theta_B$ range of 2–10°.

Table 1
Basic physicochemical data of the $FeO_x(OH)_y$ composite, the derivatives, and reference materials

Entry	Treatment	Reactant	Specific SA ($m^2 g^{-1}$)[a]	Average pore size (Å)	Pore volume (ml g^{-1})	d_{001} or d_{100} (Å)[b]
a	Fe^{III} Composite	As-prepared	2.8	–	–	36.2
b	Anion exchanged	Formate	–	–	–	–
c		Acetate	–	–	–	20 ± 2
d		Propionate	–	–	–	20 ± 2
e		Ethanol washed	–	–	–	28 ± 1
f	423 K heated[c]	Formate	95	Micropore	0.054[d]	–
g		Acetate	230 (208)[e]	Micropore	0.10[d] (0.09)[d,e]	20 ± 2 (22 ± 2)[e]
h		Propionate	128	Micropore	0.062[d]	23 ± 2
i		Ethanol washed	170	Micropore	0.085[d]	28 ± 1
j	533 K heated[c]	Formate	81	37[f]	0.10[f]	–
k		Acetate	145	37[f]	0.14[f]	–
l		Propionate	132	50[f]	0.18[f]	–
m		Ethanol washed	68	Micropore	0.008[d]	–
Fe^{III}-montmorillonite [2]			100	–	0.067[d]	15.3
α-FeO(OH) (Kanto) [2]			16	–	<0.001	–

[a] Measured after treatment in vacuum at 423 K.
[b] On the basis of XRD.
[c] Heated in nitrogen gas flow.
[d] On the basis of *t*-plot.
[e] Measured after the sorption test in 1.0 ppm of arsenite for 12 h.
[f] On the basis of DH-plot.

3.2. Sorption/desorption isotherms

The sorption and desorption isotherms were depicted in Fig. 2A(a–c) measured for anion-exchanged $FeO_x(OH)_y$ preheated at 423 K. These isotherms belong to Type I of IUPAC classification [20]. Average pore size was in micropore range based on the *t*-plot (Fig. 2B). The isotherms for ethanol-washed sample heated at 423 K belonged to a pattern as the transition from Type I to IVb (Fig. 2A(d)) [20]. Similar H2-type hysteresis was reported for ethanol-washed Fe^{III} material prepared from Fe^{III} ethoxide and cetyltrimethylammonium bromide [11]. When the heating temperature was varied between 373 and 573 K, the specific SA reached a maximum (230 $m^2 g^{-1}$) at 423 K for acetate-exchanged sample. After 423 K-heating, the specific SA for ethanol-washed samples reached the maximum 170 $m^2 g^{-1}$. The former specific SA value changed to 208 $m^2 g^{-1}$ after the sorption test in 1.0 ppm of arsenite for 12 h (Table 1g). The limited decrease (9%) may be partial damage of microporous framework in water. The changes of pore volume and *d*-spacing after sorption test were very small: from 0.10 to 0.09 ml g^{-1} and from 20 to 22 Å, respectively (Table 1g).

Next, Fe^{III} samples were heated at 533 K. Obtained isotherms belong to Type IVb for anion-exchanged samples (Fig. 2C(a–c)). The average pore size was expanded to meso-range: 37–50 Å based on the DH-plot (Fig. 2D). For ethanol-washed sample, the dV/dR_p peak was negligibly weak (Fig. 2D(d)). Therefore, the mesopore population was negligible when carboxylate was not used. The specific SA decreased when heated at 533 K compared to corresponding samples heated at 423 K except for the propionate-exchanged one (128 → 132 $m^2 g^{-1}$; Table 1).

3.3. HR-TEM

Representative TEM images were depicted in Fig. 3 measured for acetate-exchanged $FeO_x(OH)_y$ and the 423 K-heated one. Irregular distribution of thin contrast spots was observed in both images with the size of a few nanometers. The image (a) suggested totally amorphous nature. In image (b), the surface section began to form crystalline phase, and major bulk section seemed to remain as amorphous.

3.4. FT-IR

FT-IR spectra measured for $FeO_x(OH)_y$ composite and the derivative samples were depicted in Fig. 4. Obtained ratios of Fe^{III} phases and anions were summarized in Table 2. The molar ratio of dodecylsulfate versus Fe was evaluated to 0.14 for the $FeO_x(OH)_y$ composite in consistent with the ratio of introduced amount during the synthesis (1:7).

After carboxylates those are five molar times of dodecylsulfate in composite sample were introduced to the $FeO_x(OH)_y$ composite, the amount of dodecylsulfate was significantly decreased (Table 2b–d). The molar ratio of carboxylates incorporated in sample versus Fe was 0.19–0.42, excessive than the molar ratio of dodecylsulfate in the $FeO_x(OH)_y$ composite. When the $FeO_x(OH)_y$ composite was washed with ethanol, 25% of dodecylsulfate remained (e). In XRD measurements in the higher angle region, a broad peak centered at 35° invariably appeared for $FeO_x(OH)_y$ composite and carboxylates-exchanged samples (Fig. 1B(a, b)). The broad peak feature implied amorphous nature of the $FeO_x(OH)_y$. In summary, the exchange with

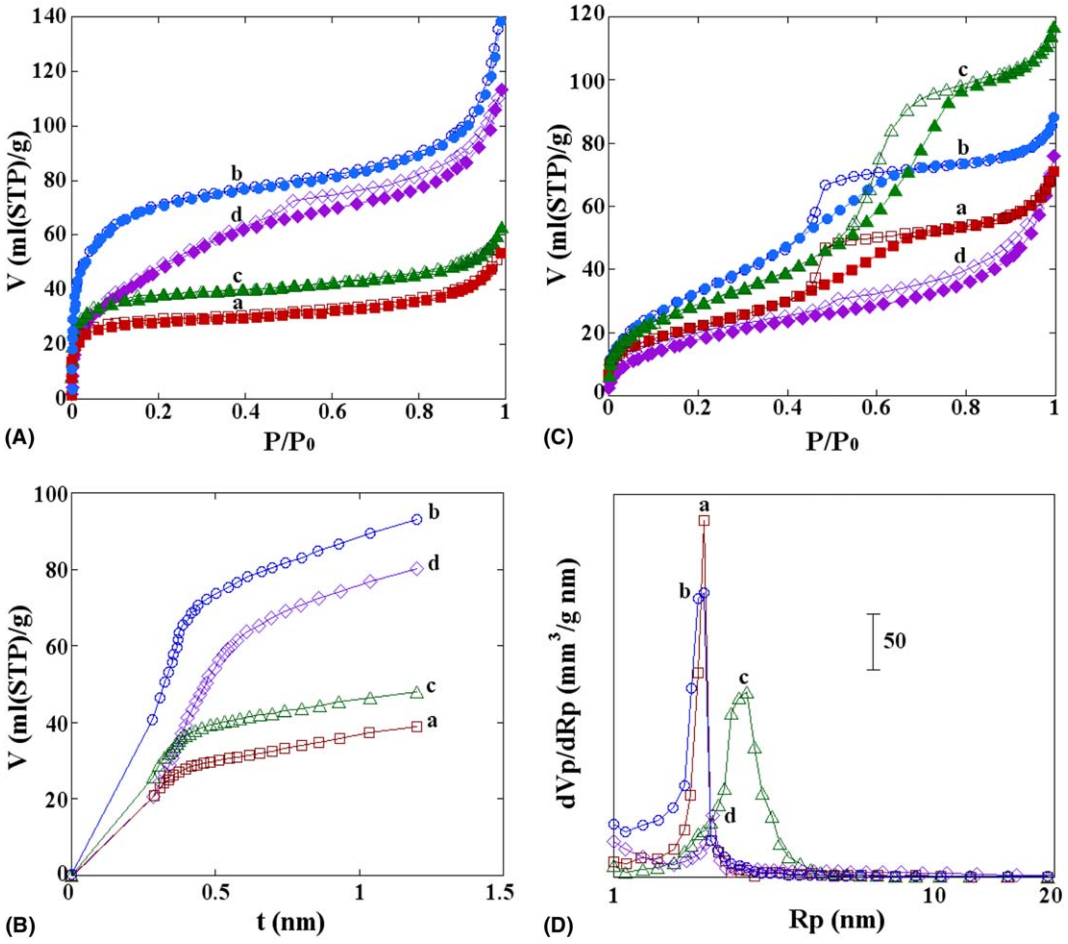

Fig. 2. (A) The sorption and desorption isotherms for exchanged $FeO_x(OH)_y$ with formate (a), acetate (b), and propionate (c) or ethanol-washed $FeO_x(OH)_y$ (d) all heated at 423 K. (B) Calculated pore size distribution based on t-plot method. (C) Corresponding samples to (A) heated at 533 K. (D) Calculated pore size distribution based on DH-plot method.

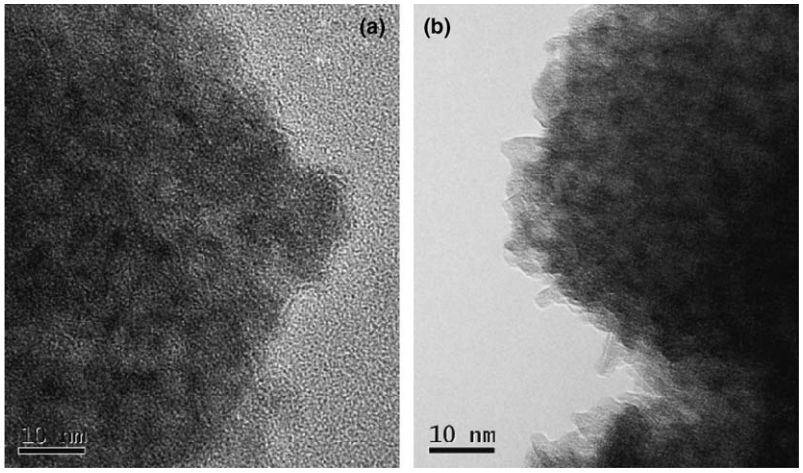

Fig. 3. TEM images for acetate-exchanged $FeO_x(OH)_y$ (a) and the one heated at 423 K in nitrogen gas flow (b).

smaller carboxylates removed most of dodecylsulfate molecules to afford micropores inside the amorphous $FeO_x(OH)_y$ framework.

When these samples were heated at 423 K, 16% of formate and 51% of acetate and propionate diminished (Table 2f–h). The molar amount of formates remained was still by

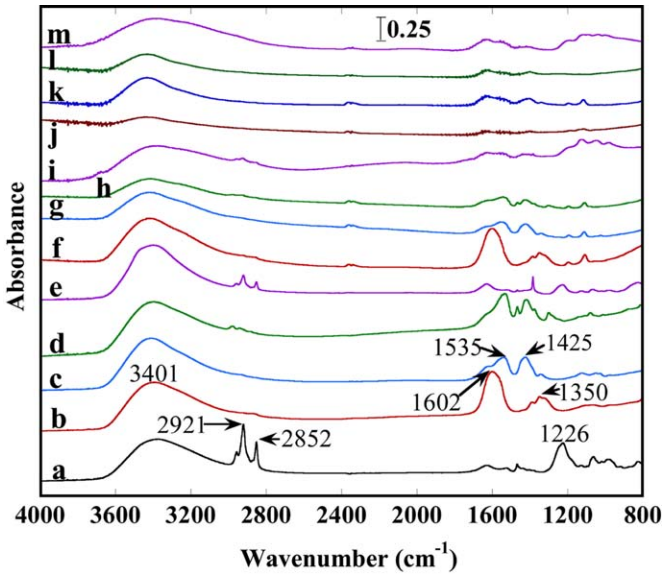

Fig. 4. (a) FT-IR spectra for $FeO_x(OH)_y$ composite (a), exchanged $FeO_x(OH)_y$ with formate (b), acetate (c), and propionate (d), ethanol-washed $FeO_x(OH)_y$ (e), and b–e heated at 423 K (f–i, respectively) or at 533 K (j–m, respectively).

2.5 times greater than that of dodecylsulfate in $FeO_x(OH)_y$ composite. The inorganic phase remained as $FeO_x(OH)_y$ because the dehydration was difficult to proceed on the internal surface of $FeO_x(OH)_y$ densely-covered with formates. In contrast, 40–60% of $FeO_x(OH)_y$ was lost for acetate/propionate-exchanged $FeO_x(OH)_y$ by heating at 423 K based on the ν_{OH} peak decrease (Fig. 4g and h). Corresponding broad XRD peak intensity at 35° became a half (Fig. 1B(b, c)). Thus, half of amorphous $FeO_x(OH)_y$ transformed into Fe_2O_3 by dehydration. The 40% of $FeO_x(OH)_y$ transformed into Fe_2O_3 for ethanol-washed one (Table 2i).

These samples were further heated at 533 K. Most of organics diminished in Table 2j–l. $FeO_x(OH)_y$ (80–50%) was lost for carboxylates-exchanged samples (Fig. 4j–l). In the XRD spectra, a set of peaks due to Fe_3O_4 crystalline was observed (Fig. 1B(d, e, f)) in contrast to the appearance of crystalline FeO(OH) phase for ethanol-washed sample (g). Remained dodecylsulfate may have decomposed until 533 K and hydrocarbon section desorbed as gas because sulfate peak at 1226 cm^{-1} remained whereas no peak remained in ν_{CH} region (Fig. 4m) [13]. Note that the values for dodecylsulfate and carboxylates in Table 2 were exclusively for intact forms of these anions. Quantitative elemental analysis should be based on ICP or EPMA measurements.

3.5. ICP and EPMA analyses for elemental compositions

The results of ICP and EPMA analyses for acetate-exchanged $FeO_x(OH)_y$ samples (as exchanged and 423 K heated) were listed in Table 3. Sulfur (0.773–0.731 wt.%) were detected in the two samples. Compared to the molar ratio dodecylsulfate/Fe^{III} of 0.14 in initial composite before acetate exchange, 18.1% and 17.7% of dodecylsulfate (or sulfur species derived from it) remained, respectively. Small amounts of Na and Cl (0.5–3.1 wt.%) were not completely washed out from the acetate-as-exchanged sample.

Assuming the exchanged molar amount of acetate/Fe^{III} of 0.19 based on FT-IR (Table 2c) and molar ratio of remained dodecylsulfate/Fe^{III} of 0.026 based on ICP, the elemental composition of acetate-exchanged $FeO_x(OH)_y$ (as exchanged) was calculated (Table 3). The calculated

Table 2
Evaluated chemical composition of Fe^{III} materials on the basis of FT-IR[a]

Entry	Treatment	Reactant	Weight (mg)				Molar ratio of ∑anion/∑Fe
			$FeO_x(OH)_y$[b]	Fe_2O_3 or Fe_3O_4[c]	Dodecylsulfate (as intact anion)	Carboxylate (as intact anion)	
a	Composite	As prepared	114	0	46	0	0.14
b	Anion exchanged	Formate	132	0	<5	28	0.42
c		Acetate	142	0	<5	18	0.19
d		Propionate	134	0	<5	26	0.24
e		Ethanol washed	147	0	15	<5	0.034
f	423 K heated	Formate	134	<10	<5	24	0.35
g		Acetate	85	(68)	<5	7	0.094
h		Propionate	60	(91)	<5	9	0.12
i		Ethanol washed	87	(63)	10	<5	≈0
j	533 K heated	Formate	29	(131)	<5	<5	≈0
k		Acetate	80	(80)	<5	<5[d]	≈0
l		Propionate	54	(106)	<5	<5[d]	≈0
m		Ethanol washed	–[d]	–	9	<5	≈0

[a] Sample weight was kept constant, 160 mg.
[b] The composition was simplified as FeO(OH) for calculations.
[c] Values indirectly obtained as the rest of Fe phases.
[d] Unknown peak exists.

Table 3
Elemental compositions of acetate-exchanged Fe^{III} materials on the basis of ICP and EPMA

Sample	Method	Weight ratio (%)							Total
		Fe	C	O	S	Na	Cl	H	
As exchanged	ICP[a]	51.88	–	–	0.773	–	–	–	
	EPMA[a]	51.4	6.7	37.0	0.80	3.1	0.5	–	100
	Calculated[b]	52.2	7.7	37.2	0.77	0	0	2.1	100
423 K-heated	ICP[a]	49.99	–	–	0.731	–	–	–	

[a] The contribution of sorbed water (19.0 wt.% in sample) was subtracted based on the sample weight change before/after vacuum (10^{-6} Pa) treatment at 290 K for these samples.
[b] Assuming acetate/Fe molar ratio of 0.19 based on FT-IR and dodecylsulfate/Fe molar ratio of 0.026 based on ICP. Simplified composition FeO(OH) was also assumed.

values were well in accord with the analyzed values using EPMA.

3.6. TG–DTA

TG–DTA data was measured for acetate-exchanged $FeO_x(OH)_y$ sample (Fig. 5). Gradual weight decrease was observed between 290 and 500 K due to the desorption/decomposition of acetate and dehydration of $FeO_x(OH)_y$. Then, abrupt weight decrease between 500 and 580 K was associated with exothermic peak. Within this temperature range (533 K), the transition of amorphous $FeO_x(OH)_y$ to Fe_3O_4 was observed in the XRD spectra (Fig. 1B).

3.7. Fe K-edge EXAFS

The EXAFS spectra were measured for $FeO_x(OH)_y$ composite, acetate-exchanged $FeO_x(OH)_y$, the one heated at 423 K, ethanol-washed $FeO_x(OH)_y$, and the one heated at 473 K. In all the Fourier-transform spectra (Fig. 6b), strong peak appeared at 1.5–1.6 Å (phase shift uncorrected) due to the Fe–O bond. A medium peak at 2.7–2.8 Å (phase shift uncorrected) was clearly observed due the Fe···Fe interaction.

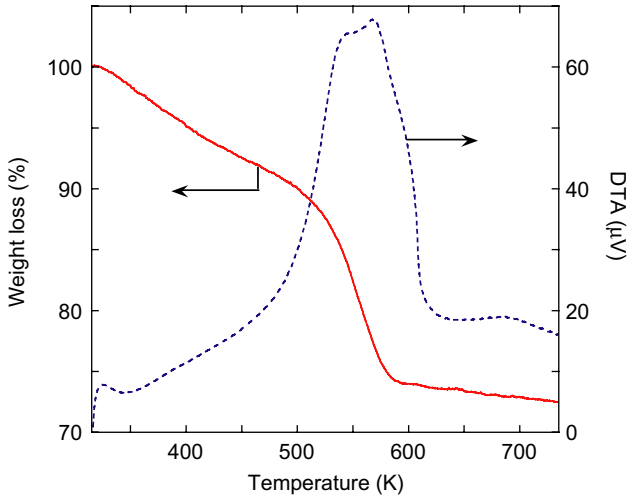

Fig. 5. TG–DTA data measured for acetate-exchanged $FeO_x(OH)_y$ in air. The ramping rate 4 K min^{-1}. TG (solid line) and DTA (dotted line) curves.

For crystallines α-Fe_2O_3, α-FeO(OH), and γ-FeO(OH), the Fe–O bond distance was between 2.0305 and 2.034 Å and the coordination number N_{Fe-O} was 6 for the octahedral [FeO_6] coordination [2,21]. Obtained Fe–O bond distance $FeO_x(OH)_y$ composite and the derivative microporous Fe^{III} materials were between 2.043 and 2.088 Å, slightly relaxed from those for standard compounds (Table 4). Associated N_{Fe-O} values fell within 4.6–6.0. Relatively smaller value (4.6) given for acetate-exchanged $FeO_x(OH)_y$ may be because of less complete array of [FeO_6] units due to highly dispersed microporous nature and/or surface reduction by acetate or ethanol. The $R_{Fe\cdots Fe}$ values also elongated (3.213–3.245 Å) compared to the value for γ-FeO(OH) (3.066 Å). These values were within the range of Fe···Fe distance for edge-shared [FeO_6] units (2.97–3.28 Å) [21]. Obtained $N_{Fe\cdots Fe}$ values (1.8–3.1), suggesting highly dispersed, unsaturated nature of microporous Fe^{III} materials.

In summary, Fe K-edge analyses demonstrated that Fe^{III} materials studied consisted of edge-shared [FeO_6] octahedral units and the unsaturated nature.

3.8. Arsenite sorption tests

Two porous Fe^{III} samples of highest specific SA were chosen. Sorption tests using our Fe^{III} porous materials in groundwater collected in Kalalanwala (Pakistan), wherein mysterious disease due to arsenic in drinking water is serious [22], are reported elsewhere. The superiority of sorption capacity varied dependent on the equilibrium dissolved arsenite concentration range (Fig. 7). When it was lower than 1.3 ppm, the superiority order was acetate-exchanged $FeO_x(OH)_y \gg$ ethanol-washed $FeO_x(OH)_y >$ Fe-montmorillonite [2] > α-FeO(OH) [4]. The first two samples were preheated at 423 K. This is plausible condition for application because the environmental regulation of As concentration is 10 ppb [1].

When the concentration was higher than 2.6 ppm, the order was acetate-exchanged $FeO_x(OH)_y \gg$ α-FeO(OH) > ethanol-washed $FeO_x(OH)_y \approx$ Fe-montmorillonite. The different trend was due to the difference of equilibrium sorption constant: 1.0×10^7 (acetate-exchanged $FeO_x(OH)_y$) $\gg 2.0 \times 10^6$ (ethanol-washed $FeO_x(OH)_y$) > 1.4×10^6(Fe-montmorillonite) > 6.4×10^5 ml g_{As}^{-1} (α-FeO

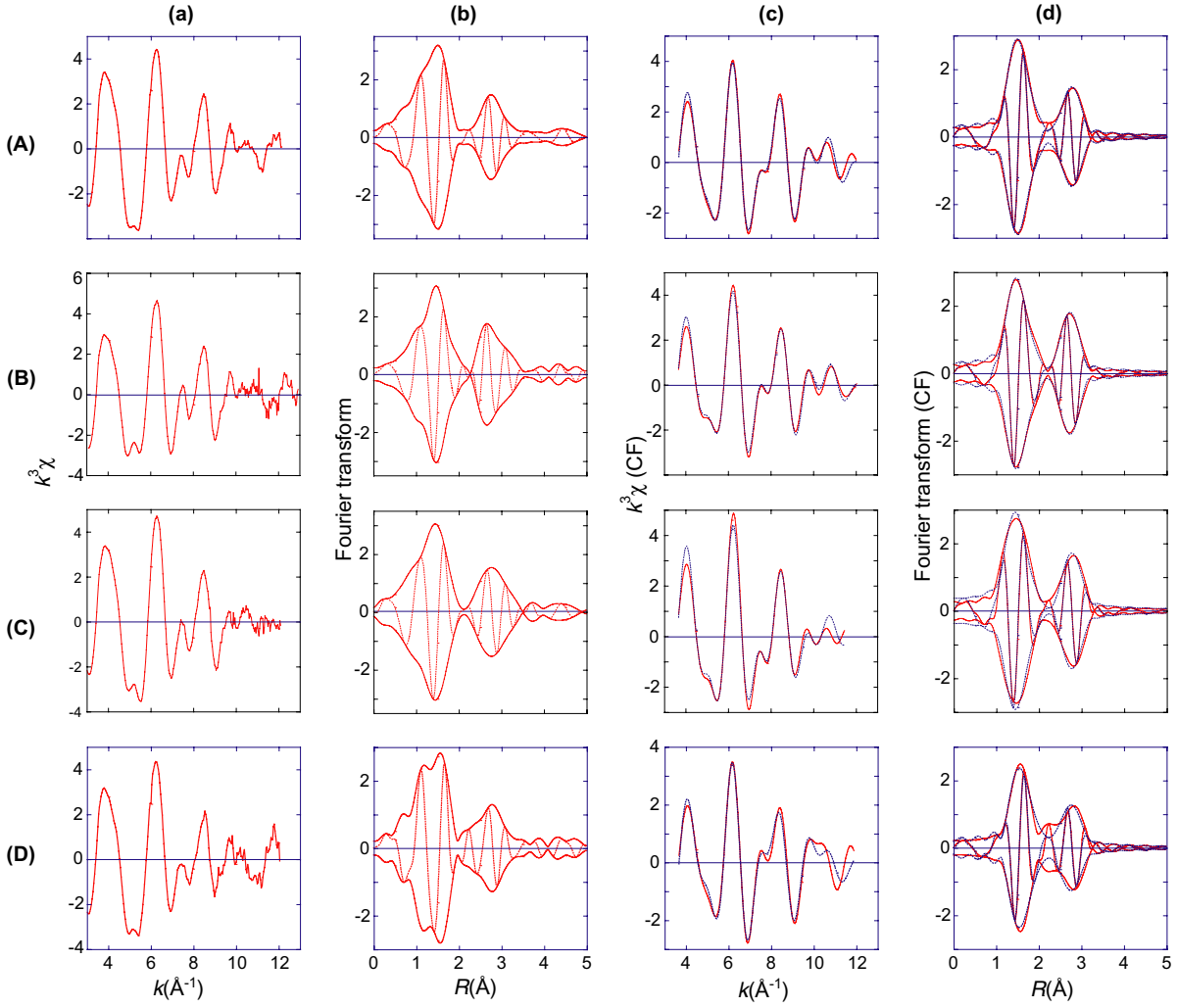

Fig. 6. Fe K-edge EXAFS spectra measured at 290 K for $FeO_x(OH)_y$ composite (A), acetate-exchanged $FeO_x(OH)_y$ (B), B heated at 423 K (C), and ethanol-washed $FeO_x(OH)_y$ (D). (a) k^3-weighted χ function, (b) its associated Fourier transform (solid line: magnitude, dotted line: imaginary part), and curve-fit analysis to the inversely Fourier-filtered $k^3\chi$ function in k- (c) and R-space (d) (solid line: experimental, dotted line: calculated).

Table 4
Best fit results of Fe K-edge EXAFS for $FeO_x(OH)_y$ composite and the derivative porous materials[a]

Sample	k-range for fit (Å^{-1})	R-range for fit (Å)	Fe–O				Fe···Fe				Goodness of fit
			N	R (Å)	ΔE_0 (eV)	$\Delta\sigma^2$ (Å^2)	N	R (Å)	ΔE_0 (eV)	$\Delta\sigma^2$ (Å^2)	
$FeO_x(OH)_y$ composite	3.7–12.0	1.11–3.13	6.0 (±0.8)	2.070 (±0.013)	−1.0 (±1.0)	−0.0002 (±0.0007)	1.8 (±0.2)	3.245 (±0.003)	−1.0 (±0.5)	0.0009 (±0.0003)	198
Acetate-exchanged $FeO_x(OH)_y$	3.7–12.0	1.14–3.08	4.6 (±0.6)	2.065 (±0.005)	0.0 (±1.1)	−0.0009 (±0.0004)	2.5 (±0.4)	3.213 (±0.020)	0.4 (±3.4)	0.0022 (±0.0007)	141
Acetate-exchanged $FeO_x(OH)_y$ heated at 423 K	3.7–11.6	1.09–3.15	5.6 (±0.5)	2.043 (±0.005)	1.9 (±0.9)	0.0010 (±0.0002)	3.1 (±0.2)	3.241 (±0.013)	−2.1 (±2.0)	0.0049 (±0.0003)	264
Ethanol-washed $FeO_x(OH)_y$	3.7–11.9	1.11–3.10	5.1 (±1.6)	2.088 (±0.027)	−7.0 (±3.5)	−0.0027 (±0.0031)	2.6 (±0.1)	3.233 (±0.011)	−0.3 (±1.4)	0.0047 (±0.0005)	136
α-Fe_2O_3[b]			6	2.0305			7	3.1293			
α-FeO(OH)[b]			6	2.021			2	3.015			
							6	3.390			
γ-FeO(OH)[b]			6	2.034			6	3.066			

[a] Values in parenthesis are estimated fit errors.
[b] From Refs. [17,18].

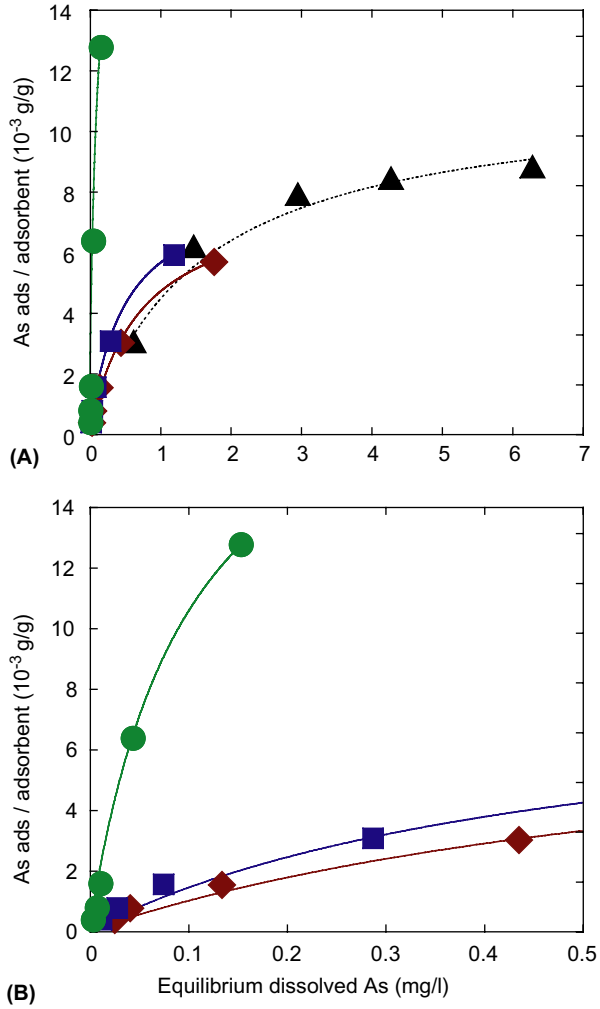

Fig. 7. Sorption isotherms of arsenite at 290 K on acetate-exchanged $FeO_x(OH)_y$ heated at 423 K (specific SA 230 $m^2 g^{-1}$; ●), ethanol-washed $FeO_x(OH)_y$ heated at 423 K (specific SA 170 $m^2 g^{-1}$; ■), Fe^{III} nanoparticles intercalated between montmorillonites (14 wt.% Fe, specific SA 100 $m^2 g^{-1}$; ◆) [2], and α-FeO(OH) (specific SA 54 $m^2 g^{-1}$; ▲) [4]. The data were plotted as points and the fits to first-order Langmuir-type equation were drawn as lines.

(OH)) evaluated assuming the first-order Langmuir-type dependence. Thus, practical superiority of acetate-exchanged $FeO_x(OH)_y$ was evident.

4. Discussion

4.1. Lamellar and reorganized microporous $FeO_x(OH)_y$

Three peaks appeared in the lower angle range of XRD for $FeO_x(OH)_y$ composite (Fig. 1A(a)) as a typical pattern of lamellar-structure [5–7]. A broad peak at 35° suggested amorphous nature of the $FeO_x(OH)_y$ (Fig. 1B(a)). The *d* spacing was calculated to 36.2 Å (Table 1a) similar to reported values for lamellar-structure formed using dodecylsulfate (35.2 Å [5] and 36.6 Å [6]). The length of a dodecylsulfate anion is ≈17.4 Å [6]. Thus, about half of the length for dodecylsulfate may interdigitate to form double layer of surfactant [6] (Fig. 8a).

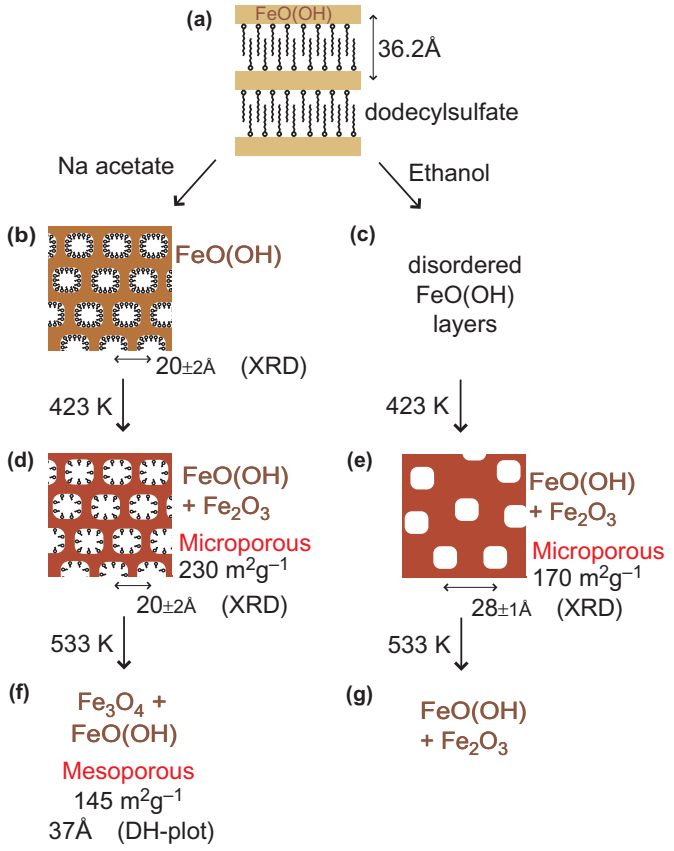

Fig. 8. Proposed structure transformation from lamellar-type $FeO_x(OH)_y$ composite to acetate-exchanged/ethanol-washed micro/mesoporous $Fe^{III/II}$ materials.

Dodecylsulfate (82%) was exchanged with formate, acetate, or propionate in ethanol. In addition to exchange reactions, extra amount of carboxylate anions (210–41%, Table 2a–d) may be exchanging with the hydroxyl groups of $FeO_x(OH)_y$. The XRD peak for acetate- and propionate-exchanged $FeO_x(OH)_y$ corresponded to *d* spacings of 20 ± 2 Å (Fig. 1A). Thin spots of a few nanometers were observed in TEM (Fig. 3a). Thus, microporous structure [9–12] adsorbed with carboxylate anions was proposed (Fig. 8b). The $FeO_x(OH)_y$ was amorphous based on broadness of the XRD peak at 35° (Fig. 1B(b)).

When the $FeO_x(OH)_y$ composite was washed with ethanol, 24% of dodecylsulfate remained. Due to the lack of organized surfactant layer, the piling regularity of inorganic layers was seriously lost judging from the broadness of (001) diffraction peak (Fig. 1A(e)). The centers were difficult to determine corresponding to the (002) and (003) peaks.

4.2. Heating to create micro and mesopores

When samples were heated at 423 K, 51% of acetate and propionate diminished (Table 2g and h). Based on the ν_{OH} peak intensity, 40–60% of $FeO_x(OH)_y$ transformed into Fe_2O_3. The molar amount of transformed Fe corresponds

to five times of acetate or propionate diminished. Thus, the dehydration of $FeO_x(OH)_y$ took place spontaneously. The inorganic phases were still amorphous based on the broadness of diffraction peaks at 35° (Fig. 1B(c)). The irregular thin contrast spots still remained after heating at 423 K in TEM (Fig. 3b). The specific SA (230 $m^2 g^{-1}$) decrease was less than 10% after the 1.0 ppm of arsenite sorption test for 12 h. The pore volume and *d*-spacing changes after the sorption test was also small (Table 1g). The adsorbed amount of arsenic was only 0.04 wt.% of sorbent in one run of sorption test and the sorption capacity negligibly changed in five consecutive sorption tests in 1.0 ppm of arsenite. Thus, the stability of this microporous structure was demonstrated for the application of As removal and repeated use.

In summary, by utilizing dodecylsulfate and subsequent acetate/propionate exchange, lamellar-structure effectively reorganized into microporous structure (Fig. 8d). A half of the carboxylates diminished by the heating at 423 K and micropores were created.

Mesostructured Fe^{III} materials were directly synthesized from Fe^{III} and palmitic or lauric acids. The mesostructure with *d* spacings of 30.8 and 24.5 Å, respectively, collapsed at 423 K in air or oxygen [10]. The Fe^{III} framework using directly carboxylates may be less stable or the heating in oxidative atmosphere (heating in nitrogen in our work) destabilized the framework.

When the ethanol-washed $FeO_x(OH)_y$ was heated at 423 K, microporous framework was formed and the specific SA was 170 $m^2 g^{-1}$ (Table 1). Via the synthesis from $Fe^{III}Cl_3$ and hexadecylsulfonate followed by washing with methanol and propanol, specific SA of 262 and 236 $m^2 g^{-1}$ were reported, respectively [7].

When these samples were heated at 533 K, the isotherms pattern changed from Type I to Type IVb (Fig. 2A and C). When most of the organics were removed, inorganic framework was lost. The average pore size was 37–50 Å for carboxylate-exchanged ones (Fig. 8f). In XRD, the peak at 35° switched into Fe_3O_4 crystalline peaks (Fig. 1B(d–f)). 80%, 50%, and 70% of $FeO_x(OH)_y$ seemed to transform into Fe_3O_4 for formate-, acetate-, propionate-exchanged samples, respectively, via the following exothermic reaction (Fig. 5)

$$R-COO^-(\text{adsorbed}) + 3FeO(OH) \rightarrow ROH + CO_2 + H_2O + Fe_3O_4\,(R = H, Me, Et) \quad (1)$$

The amount of carboxylate anions (0.42, 0.19, and 0.24 versus the amount of Fe) was sufficient to form Fe_3O_4 via Eq. (1) (Table 2). The reduction of Fe^{III} to Fe^{II} by acetate was reported for Fe^{III} hydroxoacetate heated in N_2 gas above 523 K [23].

Only very weak peak was observed in hydroxyl stretching region for formate-exchanged sample heated at 533 K (Fig. 4j). Therefore, in general for the FT-IR measurements in this work, the contribution of adsorbed water should be minor compared to that of iron oxyhydroxide. The weight loss by heating up to 723 K was 27.5% for acetate-exchanged $FeO_x(OH)_y$ by TG analysis (Fig. 5). Because the acetate contents and the weight loss due to the transformation from FeO(OH) into Fe_3O_4 are 11.3% and 13.1%, the rest of 3.1% may be due to adsorbed water.

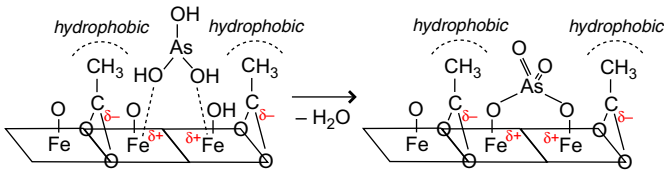

Fig. 9. Proposed promoted sorption mechanism of low concentrations of arsenite on acetate-exchanged $FeO_x(OH)_y$ heated at 423 K.

4.3. Responsible sites for optimized arsenite sorption

The arsenic uptake on Fe oxyhydroxides was correlated to the adjacent apexes of edge-sharing [FeO_6] units [2,24,25]. The Fe···Fe coordination number (1.8–3.1) was smaller for $FeO_x(OH)_y$ composite and the derivative Fe^{III} materials compared to those for standard Fe^{III} compounds (Table 4). The Fe site information deduced from EXAFS was basically common for all the Fe^{III} materials studied in contrast that the acetate-exchanged $FeO_x(OH)_y$ preheated at 423 K exhibited exceptionally excellent sorption performance for arsenite (Fig. 7). Both the saturated sorption amount (21 $mg_{As}\ g^{-1}_{adsorbent}$) and the equilibrium sorption constant (1.0×10^7 ml g^{-1}_{As}) were by far greater than ethanol-washed $FeO_x(OH)_y$, Fe-montmorillonites, and conventional bulk crystalline FeO(OH) [2,4].

Thus, the reason of this superiority seems not the formation of specific adsorption FeO_x sites for arsenite uptake. Plausible explanations may be (1) the high specific SA, microporous framework separated by 20 ± 2 Å in average (Fig. 8d, pore size ≈10 Å based on semi-quantitative *t*-plot analysis) was advantageous for the diffusion of $As(OH)_3$ (maximum molecular size 6.8 Å [26] taken van der Waals radius into account) in water, (2) adsorbed acetate inside the micropores (a half of exchanged acetate left after heating at 423 K) (Table 2) effectively exchanged with $As(OH)_3$, and (3) adsorbed acetate molecules promoted the adsorption of $As(OH)_3$ (surface site segregation by hydrophobic effect of alkyl groups, electrostatic effect, etc.) (Fig. 9).

5. Conclusions

The lamellar-structure of $FeO_x(OH)_y$ coupled with dodecylsulfate double layers reorganized to wormhole-like microporous structure stabilized with adsorbed carboxylate anions. Upon heating at 423 K, a half of acetate/propionate anions diminished and the specific surface area grew to 230–128 $m^2 g^{-1}$. The inorganic framework consisted of amorphous $FeO_x(OH)_y$ and dehydrated Fe_2O_3. This preparation method to exchange with smaller carboxylates was found to be effective to prepare microporous Fe^{III} materials

of high specific SA. The acetate-exchanged $FeO_x(OH)_y$ preheated at 423 K ($230\ m^2\ g^{-1}$) exhibited the best arsenite sorption capacity among all adsorbents that we have screened. The microporous Fe^{III} materials consisted of less complete array of [FeO_6] units based on smaller Fe···Fe coordination number (1.8–3.1). The reason that acetated-exchanged $FeO_x(OH)_y$ exhibited exceptionally excellent performance for the arsenite sorption seems not the creation of specific FeO_x surface sites. The effects of microporous framework and the presence of adsorbed acetate may be kinetically advantageous.

Acknowledgements

Fe K-edge XAFS experiments were performed under the approvals of Photon Factory Proposal Review Committee (2001G092, 2003G074, 2004G278). We are thankful for the Grant-in-Aid for Encouragement of Young Scientists from the Ministry of Education, Culture, Sports, Science, and Technology (Y.I., 1474 0401).

References

[1] P.L. Smedley, D.G. Kinniburgh, Appl. Geochem. 17 (2002) 517–568.
[2] Y. Izumi, D. Masih, K. Aika, Y. Seida, J. Phys. Chem. B 109 (2005) 3227–3232.
[3] V. Lenoble, O. Bouras, V. Deluchat, B. Serpaud, J.C. Bollinger, J. Colloid Interface Sci. 255 (2002) 52–58.
[4] S. Dixit, J.G. Hering, Environ. Sci. Technol. 37 (2003) 4182–4189.
[5] G. Wirnsberger, K. Gatterer, H.P. Fritzer, W. Grogger, B. Pillep, P. Behrens, M.F. Hansen, C.B. Koch, Chem. Mater. 13 (2001) 1453–1466.
[6] S.H. Tolbert, P. Sieger, G.D. Stucky, S.M. Aubin, C. Wu, D.N. Hendrickson, J. Am. Chem. Soc. 119 (1997) 8652–8661.
[7] L.J. Michot, C. Mathieu, E. Bouquet, Compt. Rend. Acad. Sci. IIC 1 (1998) 167–174.
[8] F. Jiao, P.G. Bruce, Angew. Chem. 116 (2004) 2–4.
[9] A. Lezau, M. Trudeau, G.M. Rsoi, L.E. Wenger, D. Antonelli, J. Phys. Chem. B 108 (2004) 5211–5216.
[10] A. Malik, M.J. Duncan, P.G. Bruce, J. Mater. Chem. 13 (2003) 2123–2126.
[11] D.N. Srivastava, N. Perkas, A. Gedanken, I. Felner, J. Phys. Chem. B 106 (2002) 1878–1883.
[12] Z. Yuan, B. Su, Chem. Phys. Lett. 381 (2003) 710–714.
[13] L. Sicard, P.L. Llewellyn, J. Patarin, F. Kolenda, Micropor. Mesopor. Mater. 44–45 (2001) 195–201.
[14] B.T. Holland, P.K. Isbester, C.F. Blanford, E.J. Munson, A. Stein, J. Am. Chem. Soc. 119 (1997) 6796–6803.
[15] J. Rasko, A. Hancz, A. Erdohelyi, Appl. Catal. A 269 (2004) 13–25.
[16] J.A. Bearden, Rev. Mod. Phys. 39 (1967) 78–124.
[17] R.L. Blake, R.E. Hessevick, T. Zoltai, L.W. Finger, Amer. Mineral. 51 (1966) 123–129.
[18] G.A. Waychunas, C.C. Fuller, B.A. Rea, J.A. Davis, Geochim. Cosmochim. Acta 60 (1996) 1765–1781.
[19] F. Schuth, Chem. Mater. 13 (2001) 3184–3195.
[20] F. Rouquerol, J. Rouquerol, K.S.W. Sing, Adsorption by Powders and Porous Solids—Principles, Methodology, and Applications, Academic Press, London, 1999, p. 199, 205, 440.
[21] R.M. Cornell, U. Schwertmann, The Iron Oxides—Structure, Properties, Reactions, Occurrence and Uses, VCH Publishers, Weinheim, 1996, pp. 12–26.
[22] A. Farooqi, N. Firdous, H. Masuda, N. Haider, Geochim. Cosmochim. Acta 67 (2003) A90.
[23] P.P.A. Filho, E.A. Pinheiro, F. Galembeck, L.C. Labaki, React. Solids 3 (1987) 241–250.
[24] B.A. Manning, S.E. Fendorf, S. Goldberg, Environ. Sci. Technol. 32 (1998) 2383–2388.
[25] J.A. Munoz, A. Gonzalo, M. Valiente, Environ. Sci. Technol. 36 (2002) 3405–3411.
[26] S.G. Kozlova, S.P. Gabuda, R. Blinc, Chem. Phys. Lett. 376 (2003) 364–369.